Hassan Marwan (Orcid ID: 0000-0001-6856-5989)

Saletti Matteo (Orcid ID: 0000-0001-5660-9200)

Zhang Chendi (Orcid ID: 0000-0001-8918-1503)

Ferrer-Boix Carles (Orcid ID: 0000-0002-5605-8979)

Co-evolution of coarse grain structuring and bed roughness in response to episodic sediment supply in an experimental aggrading channel

By

Marwan A. Hassan[1], Matteo Saletti[1], Chendi Zhang[2], Carles Ferrer-Boix[3]; Joel P.L. Johnson[4], Tobias Müller[1], Claudia vanFlotow[1]

1. Department of Geography, The University of British Columbia, Vancouver, BC, CanadaV6T 1Z2.
2. State Key Laboratory of Hydroscience and Engineering, Tsinghua University, Beijing 100084, China.
3. Department of Civil and Environmental Engineering, Technical University of Catalonia, Barcelona, Spain.
4. Department of Geological Sciences, The University of Texas at Austin, 2275 Speedway Stop C9000 Austin, TX 78712-1722

Correspondence to: Marwan Hassan, Marwan.hassan@geog.ubc.ca; phone 1-604 822 5894

This article has been accepted for publication and undergone full peer review but has not been through the copyediting, typesetting, pagination and proofreading process which may lead to differences between this version and the Version of Record. Please cite this article as doi: 10.1002/esp.4788

Running Title: Co-evolution of coarse grain structuring and bed roughness

KEYPOINTS:

- Bed surface armouring developed within the first few hours and remained intact until the end of the experiment.
- Bed structures covered around 15% of the bed surface area and were dynamic (i.e. formed, expanded, contracted and destroyed).
- Grain size, number and size of structures, and surface roughness statistics seem to vary independently of each other.

ABSTACT: We use flume experiments to better understand how gravel-bed channels maintain bed surface stability in response to pulses of sediment supply. Bed elevations and surface imagery at high spatial resolutions were used to quantify the co-evolution of surface grain-size distribution (GSD), bed roughness statistics, and bed surface structures (clusters, cells and transverse features). Using a new semi-automated method, we identified individual stone structures over a 2 m×1 m area throughout the experiments. After an initial coarsening, surface GSD and armouring ratio remained nearly stable as sediment pulses caused net bed aggradation. In contrast, individual grain structures continued to form, increase or decrease in size, and disappear throughout the experiments. The response of the bed to sediment pulses depended on the history of surface roughness evolution and bed surface structure development, as these factors changed much more in response to supply perturbations earlier in the experiments compared to later, even as the bed continued to aggrade. We interpret that the dynamic production and destruction of bed surface structures can act as a "buffer" to sediment supply pulses, maintaining a stable bed surface during aggradation with minimal change in grain size or armouring.

KEYWORDS: bedload transport, gravel bed, streams, structures, roughness, channel stability

Introduction

Accurately predicting how gravel-bed rivers respond to environmental perturbations presents many challenges for fluvial geomorphologists, aquatic scientists, engineers and land managers. Complex feedbacks among many variables are what makes the co-evolution of sediment transport rates and channel morphology—i.e. morphodynamics—difficult to predict. In gravel-bed rivers, sediment mobility is influenced by both the surface grain size distribution (GSD, also referred to as texture), and also by how surface grains become arranged and interlocked to form "structures", including clusters of coarse particles.

Bed surface texture and structures develop in response to flow conditions and sediment supply. The coarsening of bed surface GSDs relative to the subsurface or upstream supply in gravel-bed rivers is known as armouring. Experimental work has shown that the level of armouring is controlled by the flow regime (rate and duration), sediment supply (e.g., Dietrich et al., 1989), the sand content in the bed (e.g., Marion and Fraccarollo, 1997), grain-size distribution of bed material (e.g., Parker, 2008), and bed surface roughness and surface arrangements (e.g., Curran and Waters, 2014). Field observations and flume experiments suggested that bed surface armouring is destroyed during high flows (e.g., Vericat et al., 2006; Wang and Liu, 2009) resulting in the reduction of the bed armouring ratio (i.e. the ratio between the median size of the bed surface and the median size of the subsurface) and increasing sediment mobility. Other studies (Hassan and Church, 2000; Wilcock and DeTemple, 2005; Parker, 2008; Clayton and Pitlick, 2008) suggested that bed surface armouring persists even during relatively high flows implying that the channel remains relatively stable. Recently, Orru et al., (2016) conducted flume experiments to study the break up and reformation of armouring under degradational conditions. They reported that the armour surface broke up after an increase in the flow, resulting in surface fining due to the release of fine material from the subsurface. A new coarser armour layer formed quickly during the higher flow (Orru et al., 2016). In gravel-bed rivers, large grains tend to be relatively over-exposed while the smaller grains are sheltered on the bed (e.g., Kirchner et al., 1990; Hodge et al., 2013; Powell et al., 2016). "Hiding functions" model how surface GSD feedbacks enhance the mobility of coarser grains relative to finer (e.g. Parker, 1990).

Related to armouring are the bed surface structures that develop due to particle interactions and arrangements. Particle arrangements form "structures" such as pebble clusters,

ribs and stone cells (for details see Hassan et al., 2008). Previous work suggests that structures tend to be more prevalent when sediment supply is lower and beds are more stable (e.g. Church et al., 1998; Hassan and Church, 2000; Marion et al., 2003; Curran and Waters, 2014). Nonetheless, our ability to predict how bed structures will evolve under different conditions of flow, sediment supply, and GSDs remains much more limited than our ability to predict armouring. Such structures influence bed topography and surface roughness, which influence local turbulence, near-bed flow velocities and pressure gradients that transport sediment (e.g., Morris, 1955; Hassan and Reid, 1990; Nikora et al., 1998; Butler et al., 2001; Marion et al., 2003; Smart et al., 2004; Cooper and Tait, 2009; Hodge et al., 2009; Mao et al., 2011; Heays et al., 2014). They also similarly influence sediment availability, thresholds of motion, and transport rates (e.g., Brayshaw et al., 1983; Brayshaw, 1984; Dietrich et al., 1989; Church et al., 1998; Hassan and Reid, 1990; Reid et al., 1992; Hassan and Church 2000; Strom et al., 2004; Lacey and Roy, 2008; Piedra et al., 2012; Tan and Curran, 2012; Curran and Tan, 2014). Because these variables co-evolve through feedbacks, surface structures depend on the history of both the bed surface and boundary conditions (e.g. changes in discharge, sediment supply, base level) (e.g., Church et al., 1998; Hassan and Church, 2000; Parker et al., 2003; Johnson, 2017). A complete mechanistic understanding of development and dynamics of such structures in relation to flow and sediment supply regime could improve predictions of gravel bed stability, bedload transport rates, overall flow resistance, and local flow field characteristics (Dietrich et al., 1989; Church et al., 1998; Hassan and Church, 2000; Strom and Papanicolaou, 2009; Qin et al., 2017; Venditti et al., 2017). Furthermore, much of our quantitative understanding of the relation between flow intensity and sediment mass flux is based on data collected at quasi-equilibrium conditions, even though flood discharge fluctuates and sediment supply to channels is episodic.

A series of flume experiments to explore the impacts of episodic sediment supply on sediment transport, channel adjustment and sediment storage were conducted in the Mountain Channel Hydraulic Experimental Laboratory at the University of British Columbia. Based on these experiments Elgueta-Astaburuaga and Hassan (2017, 2019) and Elgueta-Astaburuaga et al. (2018) reported on the impact of episodic sediment supply on sediment transport rate, sediment transport variability, sediment mobility, sediment storage and channel adjustment. Müller and Hassan (2018) developed a numerical model to study the impact of magnitude and frequency of episodic sediment supply on channel adjustment. They used the same experiments to calibrate their numerical model. In this paper we use the same dataset to explore the evolution of gravel bed surfaces during aggradation in response to pulses of sediment supply. We document changes (e.g., formation, evolution and destruction) of bed surface structures in terms of area and density under constant flow conditions but varying sediment supply regime. Do feedbacks among these variables make them correlated and predictable, or do they evolve more independently? How much does the past history of surface evolution influence surface response to sediment supply perturbations? We answer these questions using both sediment transport data collected with a light table, and topographic data (DEMs and photos of the bed to estimate bed surface texture and structuring) collected at high temporal and spatial resolution. In addition, we present a new semi-automatic method for identifying individual grain structures.

Experimental design and methods

Experiments were conducted in an 18-m long, 1-m wide, and 1-m deep tilting flume at the Mountain Channel Hydraulic Experimental Laboratory in the Department of Geography, The University of British Columbia (Figure 1a). The initial slope was 0.0218 m/m. The upstream 6 m consisted of a fixed and immobile planar bed formed by D_{90} particles (25.8 mm; Figure 1b). The downstream 12 m of the bed consisted of well-mixed mobile sediment with an initial depth of 10 cm (the longitudinal coordinate x is equal to zero at the outlet and positive moving upstream; Figure 1a). Overall aggradation during the experiments meant that scour never reached the flume bottom. Water depth, water surface slope and bed slope were measured along the 12 m mobile bed using a mechanical point gauge with a precision of ± 0.001 m. Flow velocity was measured using ADVs in a 2 m observation reach between 6.0 and 8.0 m (Figure 1a). Water was recirculated by an axial pump. Water discharge remained constant throughout at 65 l/s, a value sufficient to fully mobilize the median size of the bed material (5.0 mm) (for

details see Elgueta-Astaburuaga et al., 2018), based on calculations using the Wong and Parker (2006) equation assuming dimensionless critical shear stress of 0.045.

Figure 1 here

Sediment was sieved in half φ intervals from 0.5 mm to 64 mm and painted in different colors for each size class for texture analysis and visual identification (Figure 1b, c). Sediment identical to the initial bulk GSD was fed into the flume at the upstream end of the mobile reach using a conveyor belt feeder (Figure 1a). The sediment transport rate and GSD at the flume outlet were measured using a light table and automated image analysis (described in Zimmerman et al., 2008; Elgueta-Astaburuaga and Hassan 2017). Material transported from the flume was trapped in a 0.25 mm mesh screen in the tailbox. Flow and sediment data are summarized in Table I and Figure 2. Overall, the experiment consisted of seven sequential 40-hour runs with differences in sediment supply (Figure 2). Runs R1 and R7 did not have additional sediment feed. Runs R2 through R6 each had the same cumulative amount of sediment supplied (300 kg), but the timing of supply varied. Runs R2 and R6 had a constant feed rate of 2 g/s for the entire 40 hours of run time. Runs R3, R4 and R5 had pulsed sediment supply: R3 had one pulse (fed in the first hour at a rate of 83 g/s), run R5 had two pulses (each fed over ½ hour at the beginning and at the 20th hour of the experiment, each at a rate of 83 g/s), and run R4 had four pulses (each fed over 15 minutes every 10 hours at a rate of 83 g/s). Additional experimental details are provided in Elgueta-Astaburuaga and Hassan (2017), Elgueta-Astaburuaga et al. (2018), and Müller and Hassan (2018).

Digital cameras mounted over the 2-m observation reach provided a fast and nonintrusive way to quantify bed surface GSD and structure in response to changes in sediment supply. We assume that measurements over this area are sufficiently representative of the entire mobile bed, consistent with our qualitative observations. Bed area close to the sidewalls was cropped. The bed surface grain size distribution was determined using the grid by number method (Wolman, 1954) by identifying particle size at the intersection of a 5 cm grid superimposed on each photograph. Individual grains were identified by color for fractions coarser than 2.83 mm. Material finer than 2.83 mm was difficult to distinguish and therefore was lumped into one size group. We measured bed surface elevation using a green laser scanner mounted on motorized cart. The sampling resolution of the bed scans was 2 mm x 2 mm with a 1 mm vertical accuracy. A 5 cm wide buffer was set on each side of the flume to avoid measurement errors associated with the walls. The DEMs of the bed were obtained from the laser scans, which were already

detrended by subtracting the slope of the flume. Both photos and laser scans were acquired after flow was stopped and the bed was allowed to dry.

Table I: Summary of hydraulics and sediment data

Notes: * sediment was fed within the first hour (300 kg/1 hour); ** sediment was fed within the first 10 minutes of each (75 kg/10 minutes); # fed within the first half an hour (150/30 minutes) – for more details see Figure 2.

Data Analyses

Bed surface structures

Although grain structures and their role in enhancing channel stability have been the focus of much research, we still lack an objective way to identify individual structures in streams and flume experiments. Relatively few attempts have been made to define and identify discrete bed structures based on variables including number of particles (Brayshaw, 1984; Hassan, 2005), identifying individual anchor stone (Brayshaw, 1984; Strom et al., 2005; Strom and Papanicolaou 2009; Hendrick et al., 2010; Heays et al., 2014), and criteria for structure shape and elevation above the bed surface. Johnson (2017) used clustering statistics to characterize the degree to which large particles were clustered, evenly spaced, or randomly distributed. This approach can give an average degree of clustering for a surface but cannot identify individual clusters.

A range of bed surface structures (called cluster types by Strom et al., 2005; Hendrick et al., 2010) has been identified in the field and the laboratory including pebble clusters, transverse lines, diamonds, rings (also called cells), upstream triangles and downstream triangles. In this work, we define structures as "*discrete, organized groupings of particles that sit above the average elevation of the surrounding bed surface*" (Strom and Papanicolaou, 2008, P. 138). We add an additional criterion that the particles must be relatively coarse compared to the bulk GSD. We propose a new multi-factor protocol to identify individual structures that are consistent with this definition. First, we visually identify all potential anchor particles ($>D_{80}$) exposed on the bed surface, representing the three largest classes of the grain size distribution (colored in blue, white and light green in Figure 3). Previous work suggests that grains of roughly that percentile tend to be anchor stones (e.g., Brayshaw, 1985; Hassan

and Reid, 1990; Strom et al., 2005; Strom and Papanicolaou, 2008; Hendrick et al., 2010; Johnson, 2017). The relative exposure (defined as the elevation of each potential anchor particle relative to the nearby bed) was evaluated using DEMs of the bed. To evaluate whether a potential anchor stone protrudes above the average local bed, we calculate the local mean bed elevation over a circle with a 64 mm radius (i.e. the b-axis of the largest particles in the distribution) centered on the potential anchor stone of interest (Figure 3). To be part of a structure, a potential anchor stone has to (i) both protrude above the mean elevation and (ii) have at least three clasts > 8 mm (corresponding to D_{60} of the bulk GSD) in contact with it, following Hassan (2005). To delineate the spatial boundary of each structure, all particles > 8 mm in contact with each other and upstream of the anchor stone were considered part of the stoss zone. Small particles (< 8 mm) downstream of each structure were identified visually and manually drawn to be included in the cluster as part of the wake zone. This method reduces the subjectivity to a few parameters (i.e., how many clasts > D_{60} need to be touching a potential anchor stone or each other to be defined as a structure, and how much an anchor stone needs to protrude) that are applied consistently to identify structures. While slightly different parameters would result in slightly different cluster distributions, our approach reduced the subjectivity in mapping bed surface structures, while being consistent with previous definitions of clusters (e.g., Hassan, 2005; Strom et al., 2005; Strom and Papanicolaou, 2008; Hentrick et al., 2010).

To examine the level of subjectivity, the analysis was done independently by three operators on one photo. Some differences were noted, but the main pattern was identical in all of them and the overall number of identified structures was very similar (± 3 structures). All our reported results were conducted by one operator, to avoid errors arising from differences among users.

Moments of the bed-elevation distribution

The first four moments (mean μ, standard deviation σ, skewness *Sk*, and kurtosis *Ku*) of the bed-elevation distribution (probability density function, PDF) for each 2-m observation reach DEM were calculated following the method in Bendat and Piersol (2000) and Coleman et al. (2011).

The Skewness of the bed-elevation distribution represents the relative shapes of positive and negative deviations from the mean bed level. A positive skewness (indicating fewer local lows and a longer tail of higher elevations) has previously been associated with water-worked and well-armoured bed surfaces (Nikora et al., 1998; Smart et al., 2004; Aberle and Nikora, 2006; Coleman et al., 2011). The kurtosis of the PDF, *Ku*, describes the variation of variance and can be thought of as the "intermittency" of larger vertical deviations. More regular bedforms with smaller spacing between them show negative *Ku*, as opposed to beds with more intermittent features and larger spacing between them, which have positive *Ku* (Aberle and Nikora, 2006; Coleman et al., 2011). Therefore, *Ku* may be a useful measure of the regularity or intermittency of the bed surface elements, i.e. micro-bedforms/structures.

Second-order structure function

Bed roughness was characterized using second-order structure function (SSF) of the DEMs to constrain the organization, orientation and scaling properties of the surface grains (Nikora et al., 1998; Aberle and Nikora, 2006; Cooper and Tait, 2009; Mao et al., 2011; Qin et al., 2017). The generalized two-dimensional second-order structure function (2DSSF), $D_b(l_x, l_y)$ of bed surface elevation $z(x, y)$ is defined as:

$$D_b\left(l_x, l_y\right) = \frac{1}{(N-n)(M-m)} \sum_{i=1}^{N-n} \sum_{j=1}^{M-m} \left\{ z\left(x_i + n\delta_x, y_i + m\delta_y\right) - z(x_i, y_j) \right\}^2 \qquad (1)$$

Where $l_x = n\delta_x$ and $l_y = m\delta_y$ are spatial lags in the streamwise (x) and transverse (y) directions, respectively; n and m are multiplying coefficients for the spatial lags; δ_x and δ_y are the sampling intervals (both are 2 mm in this study); and N and M are the total number of measured bed elevations in the streamwise and cross-stream directions, respectively.

In principle, SSFs for water-worked beds can be subdivided into scaling, transition and saturation regions (Nikora et al., 1998; Butler et al., 2001; Aberle and Nikora, 2006; Mao et al., 2011; Ockelford and Haynes, 2013). In the scaling region where spatial lags are small, the structure functions can be approximated by the power function $D_b(l_x, l_y=0)/2\sigma^2 \propto l^{2H_x}$ and $D_b(l_x=0, l_y)/2\sigma^2 \propto l^{2H_y}$ (Nikora et al., 1998). The scaling exponent H is known as the Hurst exponent, interpreted as a measure of complexity of the bed elevations (Nikora et al., 1998; Mao et al., 2011; Ockelford and Haynes, 2013). Larger values of H_x and H_y indicate a less

complex topography (Bergeron, 1996). The power function is no longer the best fit at larger spatial lags in the transition region. In the saturation region the bed surface elevations have no correlation and $D_b(l_x, l_y)/2\sigma^2$ reaches unity (Nikora et al., 1998; Mao et al., 2011). The bed surface topography can be considered randomly organized in the saturation region. The spatial lags l_{x0} and l_{y0}, which separate the scaling and saturation regions (often located in the transition region), are defined as the correlation lengths of the bed surface elevations. They can be used as the characteristic spatial scales of bed roughness, i.e. micro-bedforms or structures (Nikora et al., 1998; Aberle and Nikora, 2006; Ockelford and Haynes, 2013). Normalizing the horizontal correlation lengths by the standard deviation σ, a vertical topographic length scale for the saturation regime, provides nondimensional ratios l_{x0}/σ and l_{y0}/σ that also characterize bed roughness (Nikora et al., 1998; Ockelford and Haynes, 2013).

Results

Sediment transport and bed adjustment

Figure 2 shows the time-series of sediment transport rate at the outletfor the seven runs (for more details see Elgueta-Astaburuaga and Hassan, 2017; Elgueta-Astaburuaga et al., 2018; Müller and Hassan, 2018). R1 was conducted under zero feed conditions: at the beginning of the experiment large amounts of mostly fine gravel were evacuated from the bed surface or perhaps infiltrated between larger bed surface grains into the subsurface. Subsequently, transport rates gradually dropped by several orders of magnitude to be very low. With the start of constant feed in R2, sediment transport rates increased but remained below the feed rate, indicating net aggradation of the bed. The large sediment pulse at the beginning of R3 caused sediment transport rate to temporarily increase by 2 orders of magnitude. After 2 hours, sediment transport rate declined close to its pre-pulse value and became almost constant. For R4 and R5, trends in sediment transport were broadly similar to R3, in that sediment pulses resulted in rapid spikes in downstream transport rate, followed by gradual decay. The differences between the runs are in the magnitude of the increase in the sediment transport in response to the sediment feed pulses. R6 showed similar trends to R2 (both with constant feed) with little changes in the sediment transport rate. Although we did not feed sediment in R7, sediment availability and corresponding transport rates remained high from the abundance of bed sediment from the previous runs.

Time-series of the mean bed surface elevation and the bed surface slope are presented in Figure 4. For comparison, in Figure 4a we plot the mean bed elevation along both the flume as a whole and the smaller observation reach (e.g., 2 m). Along the observation reach, the mean bed surface elevation responded to the sediment supply regime. With no feed in R1, the bed degraded followed by a gradual aggradation during the constant feed R2 during the early stages of the run. Transport of particles initially deposited in an upstream wedge of sediment close to the channel inlet (Elgueta-Astaburuaga and Hassan, 2017; 2018; 2019) could be the cause of the sharp rise in bed elevation at the end of R2. With the episodic sediment supply, a sharp increase in mean bed elevation was observed followed by gradual decrease in the mean elevation as the sediment propagates downstream and out of the flume. Slight decline in the mean bed elevation was recorded during the time of no feed in R7. Finally, the mean bed elevation for the controlled area and the whole flume yielded similar pattern. This indicates that the observation reach responded to the sediment inputs in the same way as the whole flume. Due to the degradation pattern during R1, the bed surface slope dropped from 0.0218 to 0.0165 and then increased during R2 (Figure 4b). As in the case of the mean bed elevation, the bed responded to the episodic input of sediment by a slight increase in the bed surface slope followed by a decrease as the sediment propagate downstream. Overall, little changes in the bed surface slope were observed during runs R4-R7 (Figure 4b).

Bed surface grain size distribution

Figure 5 shows the evolution of bed surface grain size distribution over time. During R1, the bed coarsened as fine material was winnowed from the surface (Figure 5a). At the beginning of R1, the bed was well mixed, and the surface reflected the bulk GSD (Figure 5b). Most of the changes in the armour ratio were observed during the first few hours of R1; after 4 hours there was little further change in the bed surface particle size and the armour ratio (D_{50sur}/D_{50b}) ranged between 3 and 3.5 (Figure 5b). Decline in sediment transport during no feed experiments (R1, R7) is due to continued degradation of the bed and coarsening of the bed surface. During the constant feed R2, little changes in the armour ratio were observed and the inherited trend from R1 continued to dominate the textural adjustment of the bed surface. A large sediment pulse at the beginning of R3 resulted in an initial fining of the bed surface (the armour ratio dropped from 3.5 to 2.6) but then the texture of the bed surface material returned to near original values observed prior to the pulse input. The fastest and largest response was recorded for the D_{16sur}/D_{16b} ratio and the slowest and smallest for D_{90sur}/D_{90b} ratio (where the

subscripts ‘sur’ and ‘b’ refer to the surface and the bulk respectively). The response of bed surface texture to each pulse in R4 (four pulses) and R5 (two pulses) was similar to that obtained for R3 (one pulse). It is worth noting that, after 280 hours of flow and different sediment feed regimes, the armour ratio nearly matched that at the end of R1, although channel slope at the end of the experiment was approximately 17% steeper than at the end of R1 (Figure 4b).

In general, the bed surface initially fined and then coarsened after the introduction of a supply pulse. In most cases it only took around 4 hours for surface grain sizes to go back to near their pre-pulse values. Observations suggest that more of the coarse sediment remained close to the feeding point, while the fine fraction reached the observation area first and caused surface fining due to the temporal deposition of finer material (< 11 mm) on the bed surface. After the evacuation of this finer material the bed surface coarsened back to pre-pulse state.

Stone Structures

In our experiments the initial surface coarsened as fine material was winnowed away or sifted into voids between larger mobile particles during bed aggradation (Figure 4) (cf. Beschta and Jackson, 1979), but very little additional coarsening or changes in surface grain-size occurred as each run progressed (Figure 5). Flume observations showed that large particles moved short distances and typically rolled into contact with a static particle of similar size and stopped, creating surface structures. Pebble clusters were the dominant bed surface structure that developed in our experiments, followed by transverse lines and stone rings. Figure 6a shows that the development of individual structures was quite variable during the overall experiment. There did not seem to be a consistent response of structuring to sediment supply. For example, the number of surface structures increased during constant feed R2 but decreased during constant feed R6. The number of structures decreased during R3 (one large pulse) and R5 (2 intermediate pulses), but increased during R4 (four smaller pulses) (Figure 6a).

We calculate protrusion P for each point in the observation reach of the DEM as the relative elevation of that point in relation to mean elevation of the surrounding area. We used a surrounding area of 64 mm$\times$32 mm in the x and y direction respectively (calculations of

potential anchor stone protrusion that was part of the cluster identification algorithm was done differently, as described above in methods). In Figure 6c we show how mean bed protrusion evolves over time during the experiments, expressed as percentage of exceedence (e.g. a value of 5 mm for p70 means that 30% of the bed protrudes more than 5 mm compared to the surrounding area). While the 70% protrusion probability line decreases during the experiments and the others do not, responses to sediment pulses were similar. Overall, most sediment pulses caused a decrease in bed protrusion (Figure 6), presumably due to the fact that supplied sediment made the bed smoother (Figure 5a) during aggradation. Furthermore, the decrease in the bed protrusion was not significant after each pulse in R5, comparing with R3 and R4 (Figure 6). Bed surface smoothing could have contributed to render higher sediment transport rates in R6 and R7 compared to R1 and R2, respectively. This increase in bedload transport could be caused by a reduction in form drag and therefore increasing the available shear to move sediment in later runs (Figure 2). Moreover, by comparing R1-R7 and R2-R6 (same sediment supply regime), it can be seen how the last two runs show almost no change as opposed to the first two in which protrusion changed a lot. This confirms that after a complex history of sediment supply the bed reached a stable state, in which none of the morphological variables we measured changed significantly.

In these experiments with an overall aggrading bed (Figure 4), structures were dynamic. This variability is presented in Figure 7 in terms of four structure categories: newly formed, disintegrated (i.e. total destruction of the structures or most of the structure is destroyed but the anchor stone remains in place), expanded, and contracted (the structure lost particles but at least the keystone and two other particles remained). We used these categories to explore the dynamic nature of the structures (e.g., change/formation) and try to link it with the sediment supply regime. During early stages of the experiments, many new structures formed, while few disintegrated. During this period the number of contracting structures increased to a maximum immediately after the introduction of the first sediment pulse (R3). With this pulse, new and disintegrated structures also reached a maximum, but these were short lived. Contracting and expanding structures continued to be abundant, reaching a second peak toward the end of R4 (four pulses). New structures continued to develop but at an increasingly lower rate over the remaining runs. Structures disintegrated at a lower rate over this period. Overall, few structures formed or disintegrated during R7. Rates of structure expansion and contraction are generally similar after the second peak at the end of R4, declining slowly and then remaining constant for R7. These results collectively indicate that after most structures form, expansion and

contraction tend to dominate the structure dynamics. In spite of the small decline in protrusion and the number of anchored stones after R3 of about 18%, the number of surface structures during R4 increased by about 50%. The increase in the structures during R4 (Figure 6) is supported by the relatively high structural activity (expansion and contraction) during the run (Figure 7). Overall, the decline in protrusion and the number of anchored stones suggests that some structures expanded.

Statistical properties of the bed surface

The moments of the bed elevation distribution (mean, standard deviation, skewness, and kurtosis) show how surface statistics respond to changes in supply (Figure 8). The mean bed elevation increased after sediment feed (especially after the pulse at the beginning of R3), clearly demonstrating bed aggradation during R2 through R6 (Fig. 8a). The standard deviation was correlated with the range from the 95th to 5th percentile of elevation. The bed surface standard deviation showed relatively little variation overall, after increasing modestly as the bed evolved during R1 and R2. It decreased modestly immediately after sediment pulses in R4, but then recovered following each (Figure 8b and c). The standard deviation varied synchronously with D_{sur50} and D_{sur16} of the bed surface whereas D_{sur90} remained relatively stable from R3 (Figure 5a). This suggests that the adjustments of bed surface roughness height (the standard deviation) immediately following the sediment pulses were related to the fine sediments on the bed, perhaps preferentially filling in topographic lows.

Second-order structure functions

Figure 9 shows the temporal variations of the horizontal (longitudinal and transverse) correlation scales l_{x0} and l_{y0}, correlation scale ratios l_{x0}/σ and l_{y0}/σ, and the Hurst exponents H_x and H_y. Lengths l_{x0} and l_{y0} were extracted from the curves $D_b(l_x, l_y=0)$ vs. l_x and $D_b(l_x=0, l_y)$ vs. l_y, following the method of Nikora et al. (1998). After the sediment feed started in R2, l_{x0} remained larger than l_{y0}. The variation of the two correlation scales demonstrate general synchronicity (Figure 9a). The single large feed pulse at the beginning of R3 increased l_{x0} and l_{y0} initially, indicating that bed elevations became correlated over longer distances due to sediment deposition. Three of the four feed pulses in R4 resulted in smaller short-term

increases in l_{x0} and l_{y0}. However, later pulses (the third pulse in R4 and both pulses in R5) resulted in decreases in correlation length scales, indicating that increases in correlation length scales are not a universal response to sediment supply pulses. Normalized correlation scales l_{x0}/σ and l_{y0}/σ show a broadly similar pattern (Figure 9b).

H_x (mean = 0.45) was smaller than H_y (mean =0.56); this indicates that the bed topography showed a greater complexity in the streamwise than in the transverse direction. H_x tended to fluctuate more significantly than H_y, indicating more streamwise than transverse topographic sensitivity to supply perturbations. Sediment pulses in R3 and R4 tended to modestly increase H_x, indicating decrease of topographic variability along the flow direction.

Figure 10 illustrates the contour maps of SSF normalized by $2\sigma^2$ at the end of each run. The contour plot of $D_b(l_x, l_y)/2\sigma^2$ to l_x and l_y is designed to visualize the isotropy/anisotropy and alignment of the gravels or structures of various spatial scales. The contour plots of all the DEMs were generated with the maximum spatial lag in both x and y direction as ±200 mm, larger than the maximum grain size of 64 mm. The shape of the contour lines reflects the alignment and organization of the particles of different spatial scales. Although clear differences exist among the contour plots, all of them demonstrate three features: (1) Isotropy (indicated by circular rather than elliptical contours) occurred at a spatial scale similar to the grain sizes of coarse particles. The mean spatial scale at which the isotropy appeared was 26 mm, very close to the D_{90} of initial sediment mix in the flume (see Figure 1b), and smaller than but comparable with D_{90} of the bed surface (Figure 5a). (2) At spatial scales smaller than the isotropy scale (26 mm), the primary axis of the elliptical isopleths was oriented along the flow direction, suggesting anisotropy caused by a preferred alignment of the fine individual particles in the streamwise direction. (3) At spatial scales larger than the isotropy scale, the isopleths exhibit elliptical or more complex diamond-shaped isopleths (e.g. Figure 10c) but elongated transversely, which suggests anisotropy caused by clusters or micro-bedforms rested perpendicular to the flow. The distinct expansion of the contour lines at the end of R3 and R4 (e.g., contour line $D_b(l_x, l_y)/2\sigma^2$=0.60 and 0.72 in Fig. 8) shows the enlargement of grain structures or bed structures after abrupt feed regimes. It is worth noting that comparing with R3 and R4, the horizontal dimensions of grain structures decreased at the end of R5, even though two sediment pulses were fed in R5 (Figure 10f).

Discussion

Our experimental data demonstrate how an aggrading channel adjusts to changes in surface texture, structure and sediment supply. Here we separately interpret controls and feedbacks on these bed characteristics and boundary conditions in more detail.

The effect of feed magnitude

In order to compare between the sediment supply regimes, we fed the same cumulative amount of sediment (300 kg) in each run. Although the range of experimental conditions was limited, numerical simulations conducted by Müller and Hassan (2018) suggest that our results should be broadly applicable to similar aggrading fluvial systems. Müller and Hassan (2018) conducted a set of numerical simulations based on the same flume experiments presented here. They extrapolated the results by systematically varying the sediment feed characteristics to gain insight on the generalization of the results and to find thresholds of the response of the bed to different pulse frequencies and magnitudes. Their simulations show that while both the grain size distribution and the slope of the bed responded quickly to each sediment pulse, the long term adjustment of the channel to a sediment pulse regimes can be described as a balance between the fluvial evacuation capacity and the sediment pulse magnitude, frequency, and grain size distribution. In sensitivity runs they found the same relative response of the channel to a wide range of total sediment feed amounts.

Bed adjustment and armouring

Our results show that bed surface particle size responds to sediment supply within a relatively short period of time. After the initial bed surface adjustment, little changes in the armouring ratio were observed until the introduction of the next pulse of sediment (Figure 5a, b). Despite the different magnitude and frequency of the sediment feed, the armouring ratio fluctuated around 3 for most of the experiment and at the end of R7 it was nearly the same as at the end of R1 (even though the bed slope was ≈17% steeper). These results suggest that armouring ratios may dominantly reflect the source GSD from upstream, and may be largely insensitive to other perturbations and variability such as whether conditions are net aggradational or erosional, or whether sediment supply is more continuous or more episodic. Since armouring ratios adjust back rapidly after sediment supply pulses in these experiments, armouring also will not generally constrain the interval time between pulses.

Bed adjustment and sediment pulses

The bed surface adjusted to the episodic sediment pulses in different ways. We first examine the adjustments of surface grain size during R3-5. Although each pulse resulted in the clear decrease of D_{16sur} and D_{50sur}, the fining of surface grain size was more pronounced and the recovery time was longer after the single sediment pulse in R3 than with the multiple pulses in R4 and R5 (Figure 5a). The standard deviation of bed surface (Figure 8b) and the ratios of the correlation scales (Figure 9b) also demonstrate similar pattern for the variation of recovery time with the sediment supply amount (the recovery time for the pulse in R3 was about 10 h while it was about 4 h for the first three pulses in R4), which indicates that some combination of the sediment pulse magnitude and antecedent bed conditions also influence the formation of bed structures. It is noteworthy that the D_{90} of the bed surface did not show a similar difference between R3 and the other runs with abrupt sediment supply. These results suggest that the pulse magnitude affects the fining and recovery of bed surface but has limited influences on the coarse fraction of the bed surface.

We follow the analyses of Coleman et al. (2011) in our interpretations of how changes in surface skewness and kurtosis correspond to surface structure and bedform evolution after sediment pulses. Figure 8c illustrates two key features of skewness evolution. First, the skewness dropped significantly in R3 and R4 from the relatively high but fluctuating value in R1 and R2. This suggests that the sediment feed pulses in R3-4 led to a more flattened bed surface with surface structures protruding less. Second, the skewness generally increased in the second half of R5, indicating the different adjustments of bed surface with development of micro-bedforms on the bed surface. Both *Sk* and *Ku* show a sharp drop in the first 10 h of R3. *Ku* values remained relatively low, even negative in some periods during R3 and R4 (Figure 8d). This suggests that bed structures may have become more regularly spaced, with smaller spacing in between, after abrupt sediment supplies. After R4, *Ku* stayed positive and displayed a slight increasing trend until the end, indicating that the bed surface grew slightly more intermittent and the spacing between the structures increased, even under sediment pulses (R5) or constant sediment feed (R6).

The influence of sediment pulses on vertical (σ) and horizontal (l_{x0}, l_{y0}) correlation length scales of bed roughness appeared to evolve during the overall experiment. Early on, R3

and R4 sediment pulses tended to cause rapid though relatively short-lived decreases in σ. R3 caused rapid increases in l_{x0} and l_{y0}, after which these horizontal length scales tended to gradually decrease. Overall, this suggests that early sediment pulses caused a flattening of bed surface structures due to surface fining (Figure 5a) and aggradation (Figure 4a). However, the third pulse in R4 and both R5 pulses caused little change in these surface statistics, indicating that the bed morphology and texture adjusted to be less sensitive to supply. Similarly, in R6 and R7 l_{x0}/σ and l_{y0}/σ showed less fluctuation than R2 and R1, under constant sediment supply and no sediment, respectively. This again suggests that the history of sediment supply relative to flow caused the bed roughness to become more resilient to perturbations over the course of the overall experiment.

The contour plots of SSF also illustrate different patterns of bed surface adjustment between R3-R4 and R5 (Figure 11a). As with most R4 sediment pulses, the R3 pulse immediately increased anisotropy, and the primary axis of anisotropy rotated perpendicular to the flow direction. During the recovery afterwards (Figure 11b to 11c), anisotropy decreased. We interpret this to indicate a stronger influence from larger surface grains (i.e. the potential anchor stones) which the DEMs suggest tended to be arbitrarily oriented (e.g. Aberle and Nikora, 2006). In contrast, no significant difference in the bed surface alignment is found in response to the second sediment pulse in R5 (Figure 11d-f), which corresponds to the insensitive structures dynamics after this pulse (Figure 7). The two sediment pulses in R5 each introduced a larger amount of sediment than each of the four pulses in R4, but the bed surface statistics were relatively insensitive to R5. The different responses to the sediment pulses in R3-R4 and in R5 imply that episodic supplies have cumulative effects on bed surface adjustment, and therefore that the history of sediment supply regime is a first-order control on channel evolution. Modeling results reported in Müller and Hassan (2018) showed that the total sediment volume supplied was the main control on the bed slope and armouring, while the different pulse configurations only affected slope and bed surface grain sizes in the short term.

After the first pulse in R5, the D_{90sur} (Figure 5a), armour ratio (Figure 5b), standard deviation (Figure 8b) and skewness (Figure 8c) of the bed surface were all similar between R3 and R4, but the kurtosis Ku was larger and the correlation scales, l_{x0} and l_{y0}, were smaller in R5 (Figure 8d and 9a). This suggests that in R5 the bed texture was generally similar to R3 and R4 while the horizontal dimensions of bed structures were smaller and the spacing between them was larger. This might provide wider passage for the transport of fine sediment compared with

R3 and R4. Additionally, the bed slope (Figure 4b), and sediment transport (Figure 2) were all higher in R5. Therefore, the bed surface might show a higher transport capacity in R5, especially for fine sediments, although the bed structures were developed and protruding. Consequently, the abrupt R5 sediment pulse led to less aggradation (deposition depth in R4 was 4.3 mm while 3.5 mm in R5, Elgueta-Astaburuaga and Hassan, 2017).

To summarize our interpretations, the first abrupt sediment pulse resulted in larger but less protruding bed structures. Owing to the difference of transport capacity between fine and coarse grains, the coarse particles remained almost stable and acted as the anchor stones for bed structures while finer particles kept being entrained. This led to the shrinkage of bed structures and larger spacing between them, which in turn increased the transport capacity of fine particles. Consequently, the bed surface increased its stability, as it can be seen also in Figure 6c by the relative small change in protrusion (Masteller and Finnegan, 2017). We interpret that this was the mechanism for the bed surface to be increasingly insensitive and resilient to sediment pulses.

Bed adjustment without sediment pulses

Our runs indicate that the episodic sediment supply regime resulted in different adjustments of the bed surface compared to the adjustments that took place under constant sediment feed (R2 vs. R6) or no feed (R1 vs. R7). Figure 12 plots the values of *Sk* versus *Ku* of all the bed-elevation distributions. Almost all the data are located in the area referring to armoured gravel beds, as suggested by Coleman et al. (2011). Overall, changes in *Sk* versus *Ku* show that the bed surface statistics depend on the history of sediment supply over the course of the experiments. Figure 12 also exhibits the different features of bed surface under the same sediment regime before and after the sediment pulses in R3-5. The data points of R1 and R2 overlap in the plane, suggesting the similar response of the bed surface to clear water and constant sediment feed before the abrupt sediment supplies. The *Ku* increases with *Sk* for R1 and R2, which means the synchronous variation of the structure shape and intermittency (Fig. 12). In contrast, the *Ku* varied in a narrow range (most data locates in *Ku*=0.2-0.5 for R6 and *Ku* ≈0.5 for R7) while *Sk* showed more variability for both R6 and R7 (Fig. 12). The different variability between *Sk* and *Ku* results in in R6-R7 suggests that the bed structures had relatively stable spacing in between whereas fluctuating protrusion during these runs. DEMs and overhead photographs collected in R6-R7 showed that most coarse grains did not move but the entrainment and deposition of finer sediment between them kept occurring. Figure 7 also shows

that fewer new structures formed and fewer disintegrated entirely, while more changes to structures occurred through the expansion or contraction of existing stable structures. These results support the anchoring effect of the coarse grains, which helps remain the structure spacing relatively stable, and suggests that the fine sediment transport may result in shift of bed conditions during the armour process. Moreover, the asynchronism between the streamwise (x) and transverse (y) direction for the correlation lengths and correlation length ratios became distinct in R6 and R7, compared with R1 and R2 (Fig. 9a and b). This suggests that the serial abrupt sediment supplies might lead to different extensions of bed surface structures (Figure 9a). Therefore, our results illustrate that the episodic sediment pulses had accumulative effects on the evolution of bed surface structures, in terms of stability and shape, and thus, resulted in different initial bed conditions for R6 and R7 than R1 and R2.

Bed adjustment and bed surface structure dynamics

Our observations showed that structures developed, expanded and disintegrated continuously and that most structures persisted later in the experiments (Figures 6 and 7). In some cases, structures disintegrated while the anchor stone remained in place, but the same anchor stone would subsequently trap sediment and form a new structure. In other cases, the structure disintegrated and the anchor stone moved for a short distance. During the no feed runs and after the introduction of sediment pulses, structure formation and disintegration around the same anchor stone occurred sporadically, releasing relatively large quantities of sediment. Although rare, structure disintegration was most common immediately after the input of sediment pulses into the flume (Figure 7). However, no clear link was found between the pulse magnitude and the number of disintegrating structures. In our analysis we used potential anchor stones and the bed elevation data to define bed surface structures. This methodological link between structures and coarse sediment might explain their similar temporal trends of in terms of numbers and bed surface coverage. The fraction of the bed surface area covered by structures was the same at the end of R1 and R7.

Finally, the time-series of bed protrusion shows a clear response to sediment pulses: after each pulse the value of P decreases because of the filling of empty pockets in-between large grains. Moreover, P did not change much in the last two runs, confirming the general trend of stabilization of the bed detected also by the other morphological variables.

Future work

The results of our experiments showed the importance of the evolution of surface structures in response to different sediment supply regimes and provided a new method to quantify changes in grain structures. We believe that more research is needed on this subject, especially in terms of (a) exploring the pattern of surface structure dynamics in the context of bed degradation (since in our experiments the bed was overall aggrading) and with different water pulses and discharge histories, and (b) comparing different methods of quantifying stone structuring and their effect on flow resistance, sediment transport and channel stability.

Conclusions

Our results show that sediment transport rates increased substantially upon the introduction of a sediment supply pulse, but that this effect did not last long. The bed surface coarsened immediately at the beginning of the first run, when no sediment was fed into the flume. After this initial adjustment, the bed grain-size distribution did not change much for the rest of the experiment, which is shown in the temporal evolution of the median grain size and of the armour ratio. Episodic sediment pulses resulted in aggradation on the bed. Statistical analyses of the bed topography revealed the expansion and flattening of bed structures and a decrease in complexity of the bed surface overall during each feed pulse. While the bed texture did not change significantly, stone structures continued to form, evolve and be destroyed during the whole experiment. Each pulse caused the destruction of some structures but after a short period of time other structures formed. The stabilizing effect of grain structures on the bed increased during inter-pulse periods.

We surprisingly found that the different metrics and measures of bed surface topography—grain size, number and size of structures, and surface roughness statistics in both vertical and horizontal directions—seem to vary fairly independently of each other. Furthermore, the response of the bed to both constant sediment supply rate and sediment pulses varies during the experiments suggesting a strong control on antecedent topography and the "state" of the bed surface that modulates the response of structuring and bed topography to variability in sediment supply. While the lack of clear correlations between different variables limits our ability to predict how these variables will evolve, these data are useful for understanding and documenting different bed responses to fluctuating boundary conditions.

Acknowledgments

The experiment was conducted in the Mountain Channel Hydraulic Experimental Laboratory at the department of Geography, The University of British Columbia. MAH developed the idea and designed the experiment. Claudia vonFlotow, Maria Elgueta-Astaburuaga and Tobias Müller conducted the experiment. MAH, MS, CZ, TM, and CvF analysed the data and MAH, MS, CZ, CF-B, JPJ wrote the paper. The research was funded by NSERC Discovery (to M. Hassan) and Canada Foundation for Innovation (to M. Hassan). Matteo Saletti was supported by a Swiss NSF Early PostDoc Mobility Grant (P2EZP2_172206) and UBC Dean of Arts Grant (to M. Hassan). Chendi Zhang was supported by the China Postdoctoral Science Foundation (2018M641369). Eric Leinberger prepared the figures. We thank the journal editor, associate editor and two anonymous reviewers for suggestions that significantly improved the presentation. Experimental data can be found at http://doi.org/10.5281/zenodo.1227423. Additional data are available upon request from the first author.

Conflict of Interest: None of the authors has conflict of interest

References

Aberle J, Nikora V. 2006. Statistical properties of armored gravel bed surfaces. *Water Resources Research* **42**: W11414.

Bendat JS, Piersol AG. 2000. *Random Data: Analysis and Measurement Procedures*. 3rd ed., John Wiley, New York.

Bergeron NE.1996.Scale-space analysis of stream-bed roughness in coarse gravelbed streams. *Math. Geol.* **28:** 537–561.

Beschta RL, Jackson WL. 1979. The intrusion of fine sediments into a stable gravel. *J. Fish. Res. Board Can.* **36**: 204–210.

Brayshaw AC. 1984. Characteristics and origin of cluster bedforms in coarse-grained alluvial channels. In Sedimentology of Gravels and Conglomerates, Canadian Society of Petroleum Geologists, Ottawa; 77-85.

Brayshaw AC, Frostick LE, Reid I. 1983. The hydrodynamics of particle clusters and sediment entrapment in coarse alluvial channels. *Sedimentology* **30**: 137-143.

Butler JB, Lane SN, Chandler JH. 2001. Characterization of the structure of river-bed gravels using two-dimensional fractal analysis. *Math. Geol.* **33**: 301–330.

Church M, Hassan MA, Wolcott JF. 1998. Stabilizing self-organized structures in gravel-bed stream channels: field and experimental observations. *Water Resources Research* **34**: 3169-3179.

Clayton JA, Pitlick J. 2008. Persistence of the surface texture of a gravel-bed river during a large flood. *Earth Surface Processes and Landforms* **33**: 661–673.

Coleman SE, Nikora VI, Aberle J. 2011. Interpretation of alluvial beds through bed elevation distribution moments. *Water Resources Research* **47**: W11505.

Cooper JR, Tait SJ. 2009. Water-worked gravel beds in laboratory flumes - a natural analogue? *Earth Surface Processes and Landforms* **34**: 384-397.

Curran JC, Waters KA. 2014. The importance of bed sediment sand content for the structure of a static armor layer in a gravel bed river. Journal of Geophysical Research Earth Surf.**119**: 1484–1497.

Curran JC, Tan L, 2014. Effect of Bed Sand Content on the Turbulent Flows Associated with Clusters on an Armored Gravel Bed Surface. *Journal of Hydraulic Engineering* **140**: 137-148.

Dietrich WE, Kirchner JW, Ikeda H, Iseya F. 1989. Sediment supply and the development of the coarse surface layer in gravel-bedded rivers. *Nature* **340**: 215-217.

Elgueta-Astaburuaga M, Hassan MA. 2017. Experiment on temporal variation of bed load transport in response to changes in sediment supply in streams. *Water Resources Research* **53**: 763–778.

Elgueta-Astaburuaga M, Hassan MA. 2019. Sediment storage, partial transport, and the evolution of an experimental gravel bed under changing sediment supply regimes. *Geomorphology* **330**: 1-12.

Elgueta-Astaburuaga M, Hassan MA, Saletti M, Clarke GKC. 2018. The effect of episodic sediment supply on bedload variability and sediment mobility. *Water Resources Research* **54**: 6319–6335.

Hassan MA. 2005. Gravel bar characteristics in arid ephemeral streams. *Journal of Sedimentary Research* **75**: 29-42.

Hassan MA, Church M. 2000. Experiments on surface structure and partial sediment transport on a gravel bed. *Water Resources Research* **36**: 1885-1895.

Hassan MA, Reid I. 1990. Influence of microform bed roughness elements on flow and sediment transport in gravel bed rivers. *Earth Surface Processes and Landforms* **15**: 739-750.

Hassan MA, Smith B, Hogan D, Luzi D, Zimmermann A, Eaton B. 2008. Sediment storage and transport in coarse bed streams: scale considerations. In Gravel-Bed Rivers VI: From Process Understanding to River Restoration, Elsevier B.V., 473-496.

Heays KG, Friedrich H, Melville BW. 2014. Laboratory study of gravel-bed cluster formation and disintegration. *Water Resources Research* **50**: 2227– 2241

Hendrick RR, Ely LL, Papanicolaou AN. 2010. The role of hydrologic processes and geomorphology on the morphology and evolution of sediment clusters in gravel-bed rivers. *Geomorphology* **114**: 483-496.

Hodge R, Brasington J, Richards, K. 2009. Analysing laser-scanned digital terrain models of gravel bed surfaces: linking morphology to sediment transport processes and hydraulics. *Sedimentology* **56**: 2024– 2043.

Hodge RA, Sear DA, Leyland J. 2013. Spatial variations in surface sediment structure in riffle-pool sequences: a preliminary test of the differential sediment entrainment hypothesis (DSEH). *Earth Surface Processes and Landforms* **38**: 449-465.

Johnson JPL. 2017. Clustering statistics, roughness feedbacks, and randomness in experimental step-pool morphodynamics. *Geophysical Research Letters* 44: 3653–3662

Johnson JPL, Aronovitz AC, Kim W. 2015. Coarser and rougher: effects of fine gravel pulses on experimental step-pool channel morphodynamics. *Geophysical Research Letters* **42**: 8432-8440.

Kirchner JW, Dietrich WE, Iseya F, Ikeda H. 1990. The variability of critical shear stress, friction angle, and grain protrusion in water worked sediments. *Sedimentology* **37**: 647–672.

Lacey RWJ, Roy AG. 2008. Fine-scale characterization of the turbulent shear layer of an instream pebble cluster. *Journal of Hydraulic Engineering* **134**: 925–936.

Mao L, Cooper JR, Frostick LE. 2011. Grain size and topographical differences between static and mobile armor layers. *Earth Surf. Processes Landforms* **36**: 1321–1334.

Marion A, Fraccarollo L. 1997. Experimental investigation of mobile armoring development, *Water Resources Research* **33**: 1447–1453.

Marion A, Tait SJ, McEwan IK. 2003. Analysis of small-scale gravel bed topography during armoring. *Water Resources Research* **39**: 1334.

Masteller CC, Finnegan NJ. 2017. Interplay between grain protrusion and sediment entrainment in an experimental flume. *Journal of Geophysical Research* **122**: 274-289.

Meyer-Peter E, Muller R.1948. Formulas for bedload transport. In *Proceeding of the 2nd IAHR Congress*, Stockholm.

Morris HM. 1955. Flow in rough conditions. *Transaction of the American Society of Civil Engineering* **120**: 373–398.

Müller T, Hassan MA. 2018. Fluvial response to changes in the magnitude and frequency of sediment supply in a 1-D model. *Earth Surf. Dynam*. **6**: 1041–1057.

Nikora VI, Goring DG, Biggs BJF. 1998. On gravel-bed roughness characterization. *Water Resources Research* **34**: 517-527.

Ockelford AM, Haynes H. 2013. The impact of stress history on bed structure. *Earth Surface Processes & Landforms* **38**: 717-727.

Orru C, Blom A, Uijttewaal WSJ. 2016. Armor breakup and reformation in a degradational laboratory experiment. *Earth Surface Dynamics* **4**: 461-470.

Parker G. 1990. Surface-based bedload transport relation for gravel rivers. *Journal Hydraulic Research* **28**: 417–436.

Parker G. 2008. Transport of gravel and sediment mixtures. In Sedimentation Engineering. Processes, Measurements, Modeling and Practice, Am. Soc. of Civ. Eng., Reston, Va., 165–251.

Parker G, Toro-Escobar CM, Ramey M, Beck S. 2003. The effect of floodwater extraction on the morphology of mountain streams. *Journal of Hydraulic Engineering* **129**: 885-895.

Piedra MM, Haynes H, Hoey TB. 2012. The spatial distribution of coarse surface grains and the stability of gravel river beds. *Sedimentology* **59**: 1014–1029.

Powell MD, Ockelford A, Rice SP, Hillier JK, Nguyen T, Reid I, Tate NJ, Ackerley D. 2016. Structural properties of mobile armors formed at different flow strengths in gravel-bed rivers. *Journal of Geophysical Research* **121**: 1494-1515.

Qin J, Zhong D, Wu T, Wu L. 2017. Evolution of gravel surfaces in a sediment-recirculating flume. *Earth Surface Processes and Landforms* **42**: 1397-1407.

Reid I, Frostick LE, Brayshaw AC. 1992. Microform roughness elements and the selective entrainment and entrapment of particles in gravel-bed rivers. In Dynamics of Gravel-bed Rivers, John Wiley & Sons Ltd., Chichester, pp. 253-275.

Smart GM, Aberle J, Duncan M, Walsh J. 2004. Measurement and analysis of alluvial bed roughness. *Journal of Hydraulic Research* **42**: 227-237.

Strom, K.B. and Papanicolaou, A.N., 2008. Morphological characterization of cluster microforms. Sedimentology, 55 (1), 137-153.

Strom KB, Papanicolaou AN. 2009. Occurrence of cluster microforms in mountain rivers. *Earth Surface Processes and Landforms* **34**: 88-98.

Strom K, Papanicolaou AN, Evangelopoulos N, Odeh M. 2004. Microforms in gravel bed rivers: Formation, disintegration, and effects on bedload transport. *Journal of Hydraulic Engineering* **130**: 554-567.

Strom KB, Papanicolaou AN, Billing B, Ely LL, Hendricks RR. 2005. Characterization of particle cluster bedforms in a mountain stream. In Proceedings of the ASCE/EWRI World Water and Environmental Resources Congress, ASCE, Resont, Virginia, 399.

Tan L, Curran JC. 2012. Comparison of Turbulent Flows over Clusters of Varying Density. *Journal of Hydraulic Engineering* **138**: 1031-1044.

Venditti JG, Nelson PA, Bradley RW, Haught D, Gitto AB. 2017. Bedforms, Structures, Patches, and Sediment Supply. In Gravel-Bed Rivers, Gravel-Bed Rivers: Processes and Disasters, John Wiley.

Vericat D, Batalla RJ, Garcia C. 2006. Breakup and reestablishment of the armour layer in a large gravel-bed river below dams: The lower Ebro. *Geomorphology* **76**: 122–136.

Wang T, Liu X. 2009. The breakup of armor layer in a gravel bed stream with no sediment supply. In Advances in Water Resources and Hydraulic Engineering, Springer Berlin Heidelberg, 919–923.

Waters KA, Curran JC. 2015. Linking bed morphology changes of of two sediment mixtures to sediment transport predictions in unsteady flows. *Water Resources Research* **51**: 2724– 2741.

Wilcock PR, DeTemple BT. 2005. Persistence of armor layers in gravel-bed streams, *Geophysical Research Letters* **32**: L08402, doi:10.1029/2004GL021772.

Wolman MG. 1954. A new method of sampling coarse river-bed material. *Transactions of the American Geophysical Union* **26**: 951–956.

Wong M, Parker G. 2006. Reanalysis and correction of bed-load relation of Meyer-Peter and Meuller using their own database. *Journal of the Hydraulic Engineering* 132: 1159–1168.

Zimmermann AE, Church M, Hassan MA. 2008. Video---based gravel transport measurements with a flume mounted light table. *Earth Surface Processes and Landforms* **33**: 2285-2296.

Table I: Summary of hydraulics and sediment data

Run	Feed regime	Total Pulse magnitude (kg)	Pulse recurrence interval (hours)	Feed rate (g/sm)	Water depth (cm)	Water surface slope (m/m)	Bed slope (m/m)	Mean Bedload transport rate for the run (g/sm)
R1	No feed	----	----	0			0.017	1.29
R2	Constant	----	----	2	7.3	0.017	0.016	0.65
R3	One Pulse	300	40	83*	8.0	0.016	0.018	1.56
R4	4 pulses	75	10	83**	8.3	0.018	0.020	0.98
R5	2 pulses	150	20	83#	7.2	0.02	0.022	1.19
R6	Constant	----	----	2	7.5	0.02	0.022	1.25
R7	No feed	----	----	0	7.3	0.02	0.022	0.42

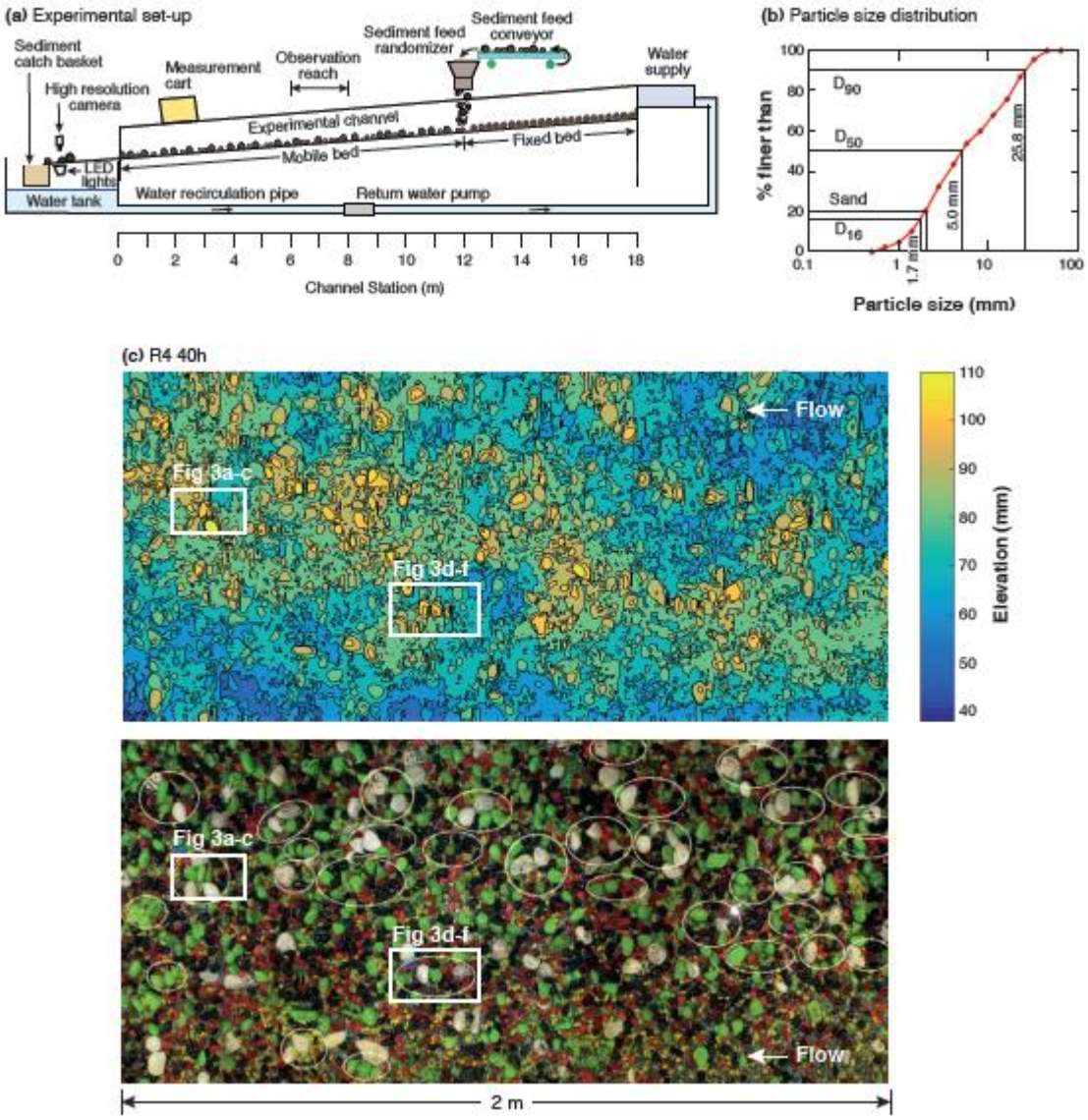

Figure 1. (a) Overview of the experimental set-up showing the locations of sediment feed, fixed bed, mobile bed, and observation reach, (b) grain size distribution of the experimental sediment, (c) an example of photograph and topographic surface of the observation reach (R4 at 40h). Circles show the location of identified bed surface structures. Labeled rectangles show the location of the structures presented in Figure 3.

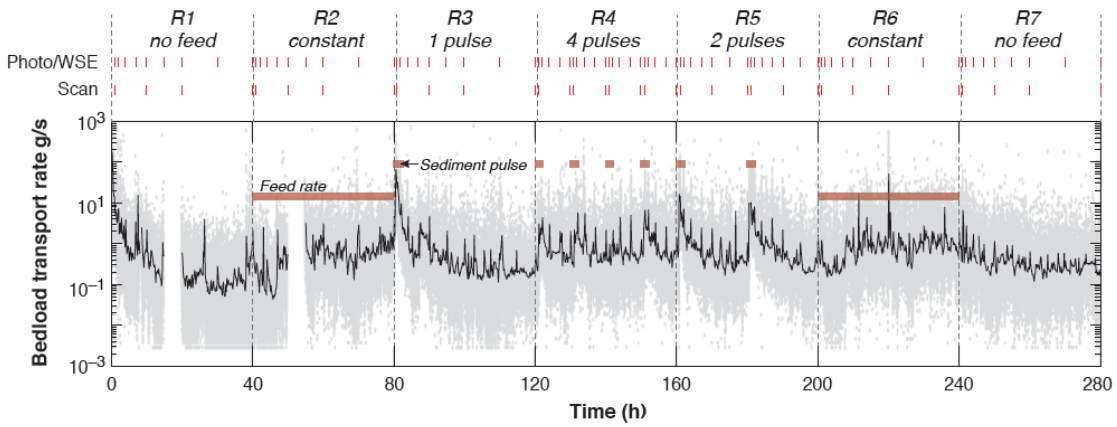

Figure 2. Experimental design and outlet sediment transport rate during runs 1-7. Red markers illustrate the time at which different measurements were done: bed surface photographs (Photo), water surface elevation and bed elevation (WSE), and bed elevation laser scans (Scan). Sediment transport rates measured every second are plotted as grey points and a ten-minute average in black.

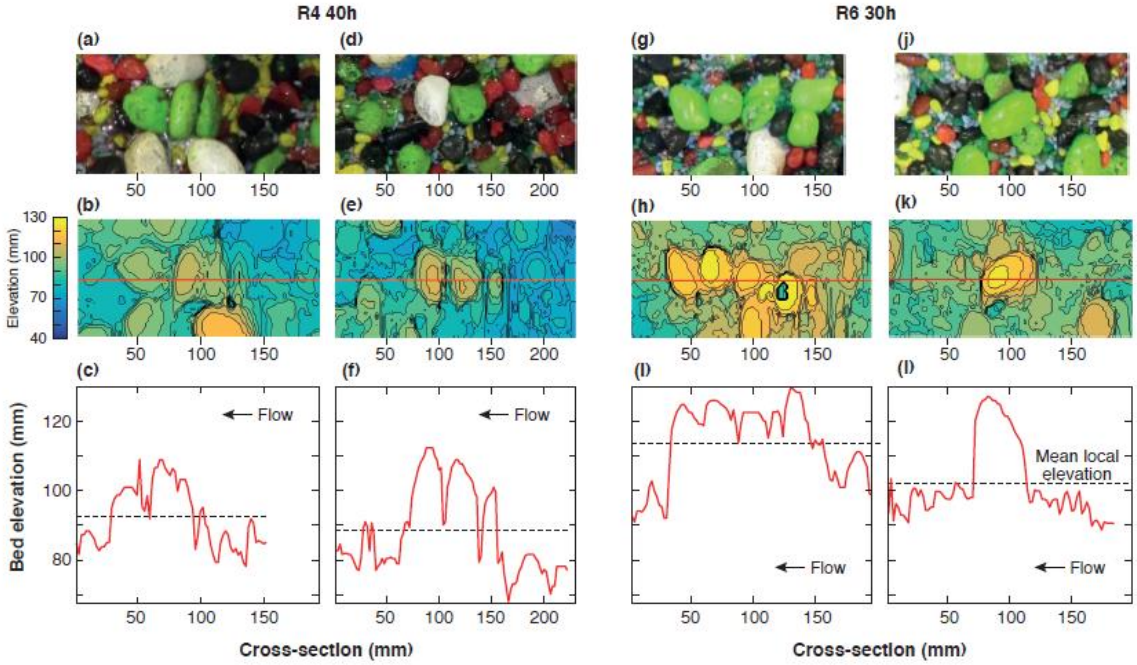

Figure 3. (a), (d) and (g) are three structures identified during the experiment. (j) Represents an example of potential anchor stone with no development of structures. Panels (c), (f), (i), and (l) represent the longitudinal profiles through the red lines in panels (b), (e), (h), and (k), which are drawn through the centroid of the potential anchor stones. Note that the structure in (a) expanded laterally from a single line structure (e.g., the white stones). Water flows from right to left.

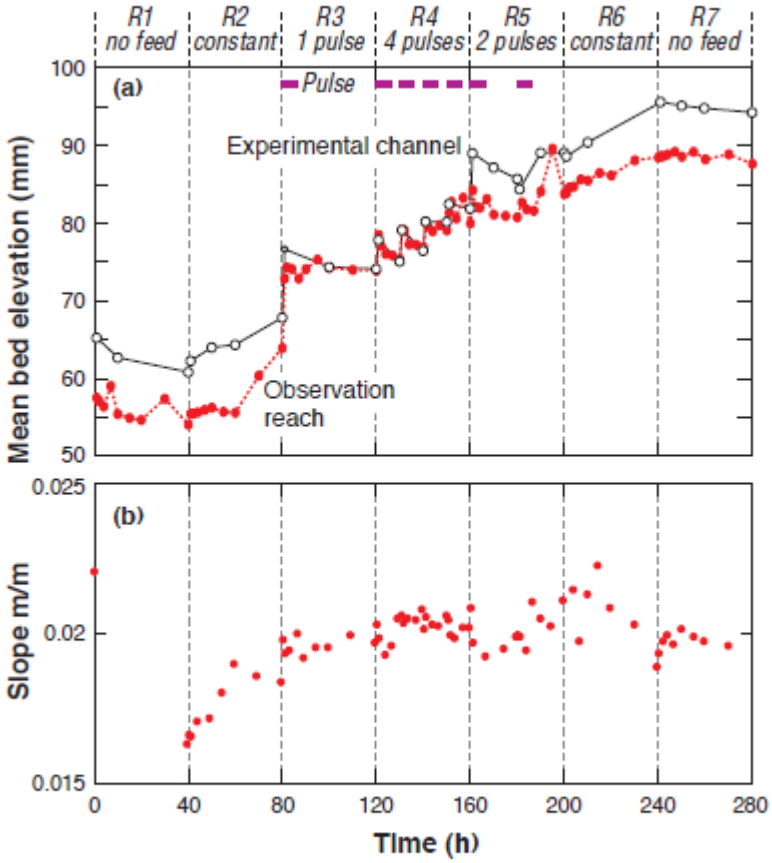

Figure 4. (a) Mean bed elevation along the entire flume (12 m) and the observation reach (2 m). Note that the first bed scan was taken at t=1 hour. (b) Temporal adjustment in the bed surface slope. The Slope was measured over the entire mobile bed (12 m). During R1 (no feed) the entire flume degraded. More sediment was eroded from upstream, causing the bed slope to drop from 0.0218 to 0.0165.

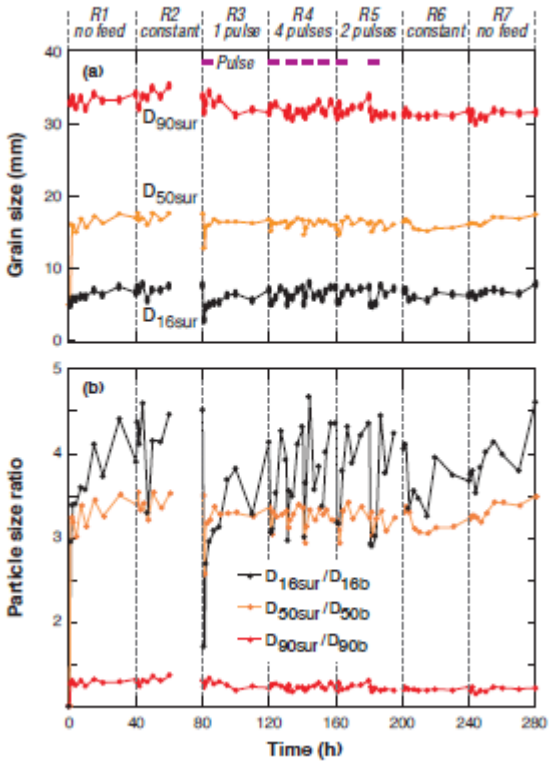

Figure 5. (a) Temporal change in the D_{16sur}, D_{50sur}, and D_{90sur} of the bed surface. (b) Temporal changes in particle size ratios of the bed surface and the bulk sediment mixture for D_{16sur}/D_{16b}, D_{50sur}/D_{50b}, and D_{90sur}/D_{90b} during the experiment (D_{16b}=1.7 mm; D_{50b}=5.7 mm, and D_{90b}=27.2). At the start of R1 (t=0), we assumed that the bed surface is similar to the mixture and therefore all values are equal to 1. Note that the first GSD measurements were taken at t = 1h, so there was time for the bed to coarsen which is reflected in the values of the D_{16sur}, D_{50sur}, and D_{90sur}.

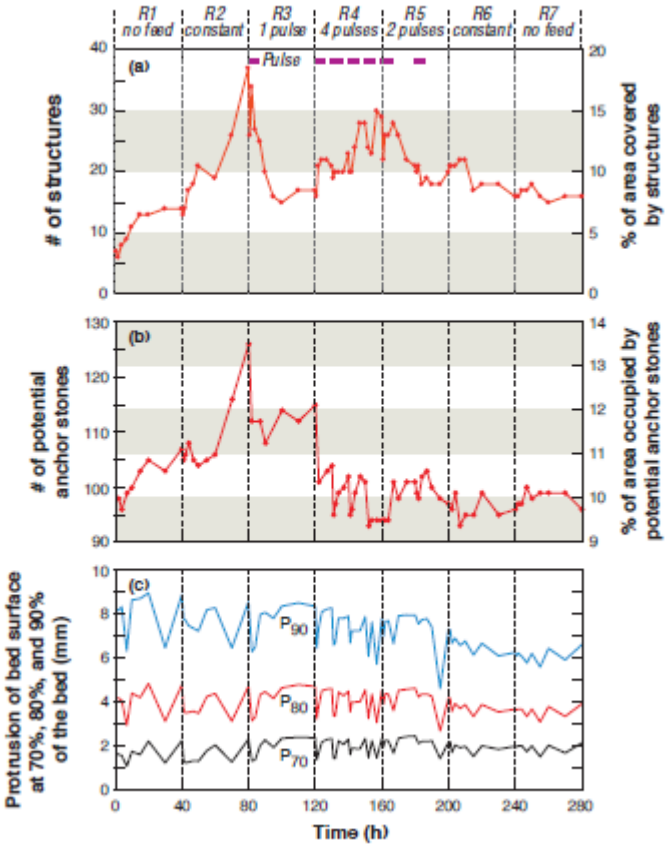

Figure 6: (a) The total number and total area covered (as a percentage of the total observation area) by identified structures, (b) Total number and total area covered by (as a percentage of the total area) potential anchor particles found on the bed surface (32-45 and 45-64 mm), and (c) Protrusion over the observation reach expressed as percentage of the bed surface (90%, 80% and 70%) below a given value evaluated over a window of 1 D_{max} (D_{max} = 64 mm) in the longitudinal direction and ½ D_{max} in the transversal direction (i.e. 64mm x 32mm).

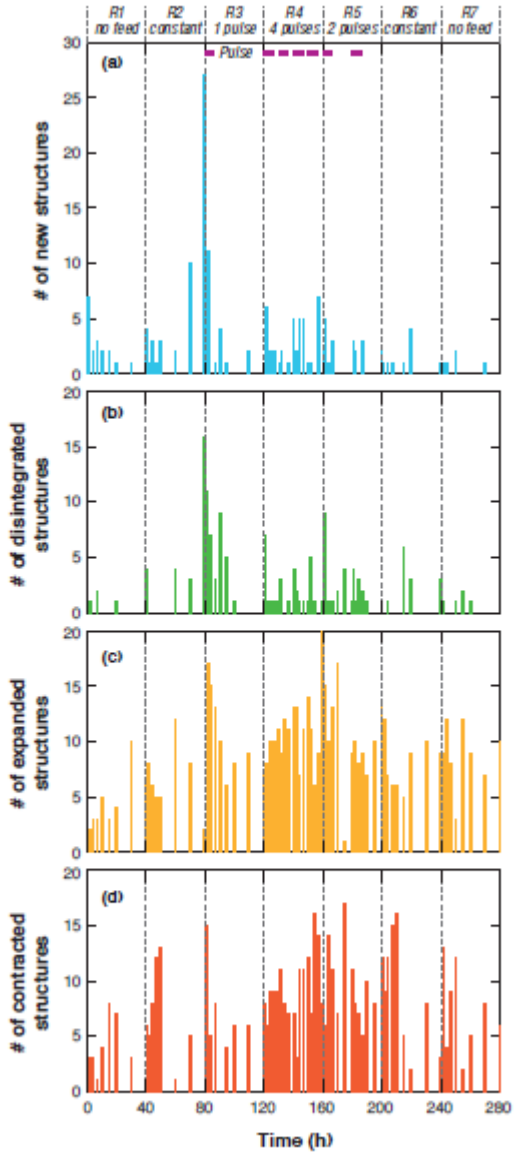

Figure 7. Total number of (a) newly formed, (b) disintegrated, (c) expanded, and (d) contracted structures during the experiment. Typically, structures that existed for at least seven hours at any point during a run would increase in surface area.

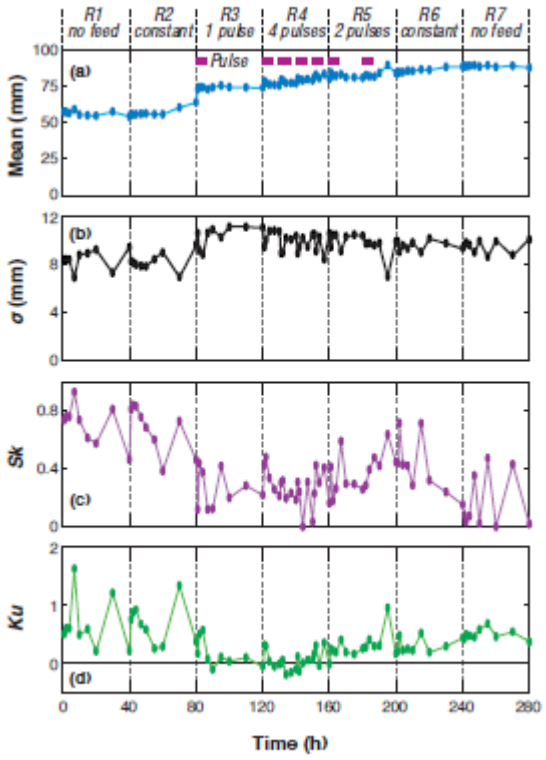

Figure 8. (a) Mean, (b) standard deviation, (c) skewness, and (d) kurtosis of the bed elevation distributions for the 2 m-long scanned bed surface during the whole experiment.

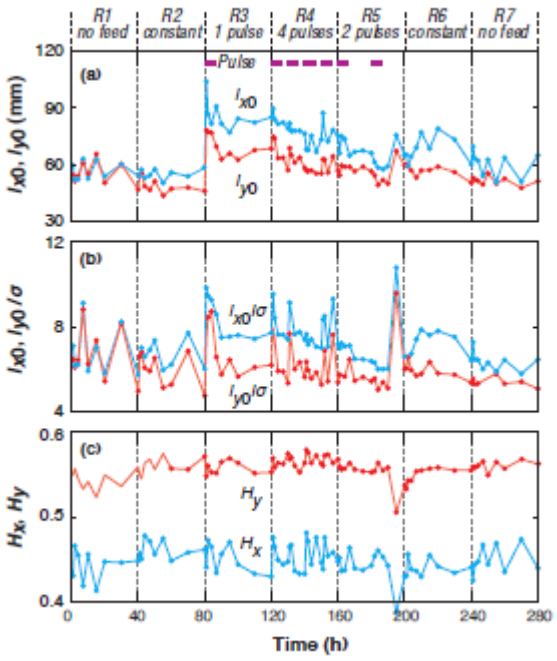

Figure 9. Temporal variation of (a) correlation scale l_{x0} in x (streamwise) direction and l_{y0} in y (transverse) direction; (b) l_{x0} and l_{y0} normalized by the standard deviation σ of the bed elevation distributions; (c) Hurst exponent for x direction and y direction.

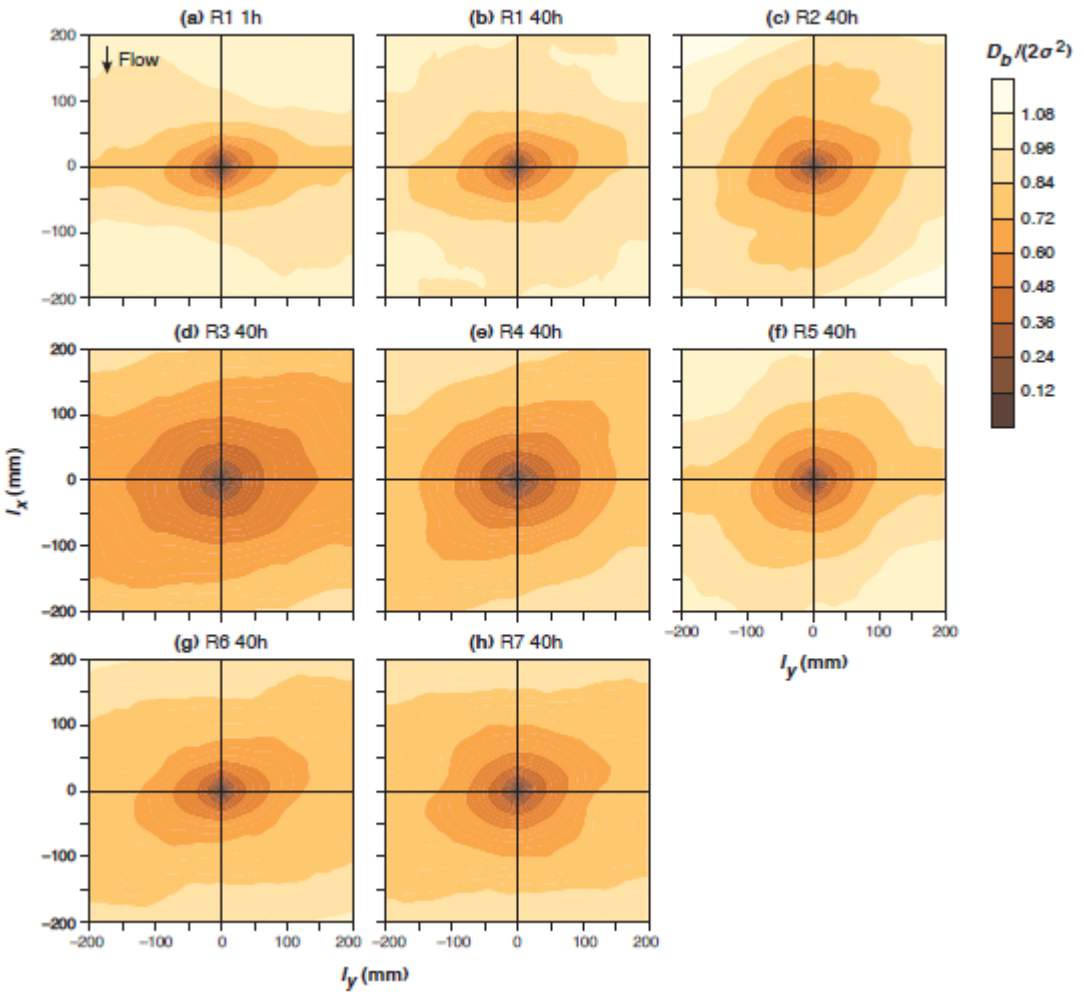

Figure 10. Isopleths maps of the two-dimensional structure functions for the 2 m-long scanned bed surface. (a) Refers to the result of the DEM at the 1st hour as the initial bed condition. (b) to (h) are the results of the DEMs at the end of each run.

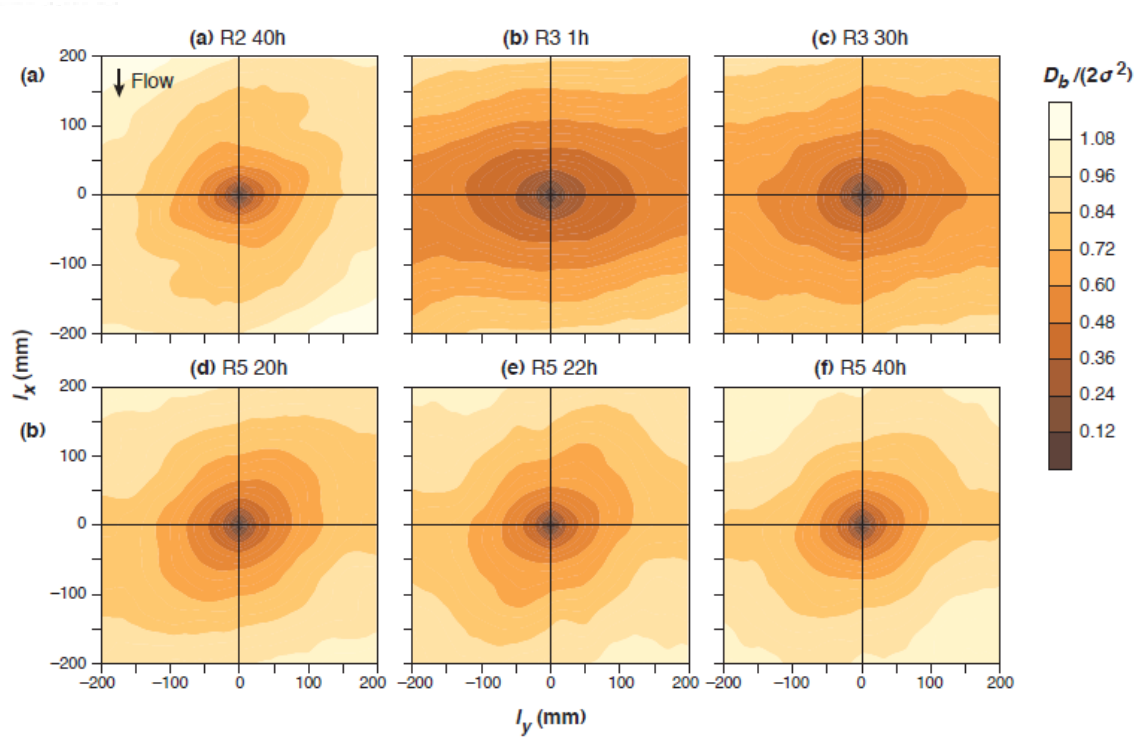

Figure 11. Isopleths maps of $D_b(l_x, l_y)/2\sigma^2$ for the influence of sediment feed pulses: (a) the sediment pulse at the beginning of R3; (b) the second sediment pulse in R5. The isopleths maps in the first column refer to the bed surface before the sediment pulse. The isopleths maps in the second and the third column depict the immediate adjustment and the grain organization before next sediment pulse or run, respectively.

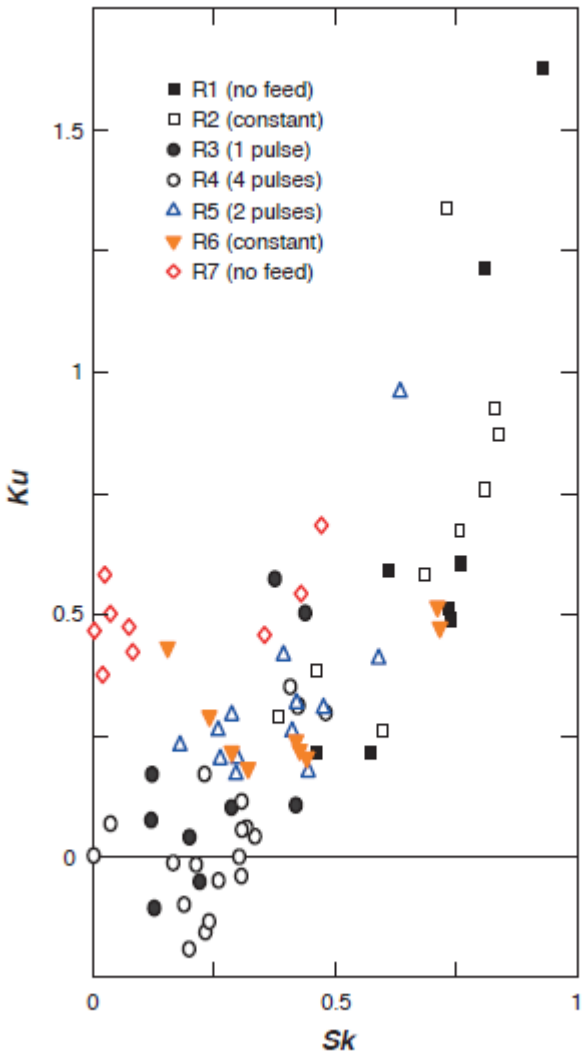

Figure 12. Changes in the *Sk-Ku* plane for all the DEMs. Data are grouped based on the feed regime. We plotted the moments of each DEM on the *Sk-Ku* plane. The vertical axis where *Sk*=0 refers to the PDF symmetric about the mean. The *Sk*>0 area of the plane indicates the bed surface with more protruding structures, while *Sk*<0 refers to greater depressions between the structures. Positive *Ku* means the bedforms or structures are more intermittent while the negative values suggest consecutive bed elements.